MASS TRANSFER CONTROL OF A BACKWARD-FACING STEP FLOW BY LOCAL FORCING-EFFECT OF REYNOLDS NUMBER

by

Zouhaier MEHREZ [a*]***, Mourad BOUTERRA*** [a]***, Afif EL CAFSI*** [a]***, Ali BELGHITH, and Patrick LE QUERE*** [b]

[a] Faculté des Sciences de Tunis, Tunis, Tunisie
[b] Laboratoire d'Informatique pour la Mécanique et les Sciences d'Ingénieur CNRS, Orsay, Cedex, France

Original scientific paper
UDC: 532.517.2/.6:536.24:66.011
DOI: 10.2298/TSCI1102367M

The control of fluid dynamics and mass transfer in separated and reattaching flow over a backward-facing step by a local forcing, is numerically studied using large eddy simulation.The control is realized by a sinusoidal oscillating jet at the step edge. The Reynolds number is varied in the range of $10000 \leq Re \leq 50000$ *and the Schmidt number is fixed at 1.The obtained results show that the flow structure is modified and the local mass transfer is enhanced by the applied forcing. The observed changes depend on the Reynolds number and vary with the frequency and amplitude of the local forcing. For all Reynolds numbers, the largest reduction of the recirculation zone size is obtained at the optimum forcing frequency St = 0.25. At this frequency the local mass transfer enhancement attains the maximum.*

Key words: *backward-facing step, large eddy simulation, mass transfer, sinusoidal forcing*

Introduction

The phenomena of separation and reattachment, involving heat and mass transfer, appear under a variety of flow condition and occur commonly in many engineering systems like gas turbine engines, heat exchangers, combustors, chemical reactors, electronic equipment, and many others applications. So, to control flow separation, many investigations by numerous authors have been conducted in fluids engineering. A widely known case is the backward facing step flow problem which continues to draw interest from CFD community because of its rich flow physics in spite of its simple geometry. As a result, it has emerged as one of the benchmark problems.

Separated flows show positive and negative effects depending on the application. A desired recirculation region as result of a separation is needed in combustion chambers to keep the fuel mixture in reaction zone for a complete combustion. By influencing a recirculation zone, the residence time behaviour in general mixing problem is altered. In contrast to that, negative consequences could be a loss in efficiency and noise production in turbo-machines or process plants such as diffusors. Thus, the suppression or desired control of

* Corresponding author; e-mail: zouhaier.mehrez@yahoo.fr

separation phenomena has been addressed in the mechanics community for many decades. There has been much research interest on the periodically perturbed turbulent separated flow. Singurdson [1], Chun *et al.* [2] are interested to the active control of the reattachment process, in which the enhancement of momentum transport across the separated shear layer plays a major role. Several authors are interested to the excitation of the instability and vortex formation inherent to the separated shear layer [3-7].

Other authors extended their research to study the effect of control on the thermal and mass transfers in the separated and reattaching flows. Among them, Oyakama *et al.* [8] showed an overall increase of heat transfer by introduction of a jet discharge from a slit located in the duct wall opposite a step. Velazquez *et al.* [9] are interested to influence of frequency and amplitude of pulsating flow behind the backward facing step. They showed that the heat transfer augment with pulsating amplitude. By application of a local periodic perturbation in the flow behind a backward facing step Mehrez *et al.* [10] demonstrated that the local heat transfer enhances. The largest enhancement is observed at the optimum Strouhal number of perturbation St = 0.25. Hwang *et al.* [11], showed that the mass transfer enhances by introduction pulsating components into the free stream over a blunt flat plate of finite thickness. Younsi *et al.* [12] showed that the application of a transverse magnetic field normal to the flow direction decreases the heat and mass transfer double diffusive flow in a trapezoidal porous cavity. Xu *et al.* [13] has performed a numerical investigation on a two dimensional pulsed turbulent impinging jet under large temperature differences between the jet flow and the impinging surface to examine the effect of temperature-dependent thermo-physical properties along with pulsation of the jet on the local Nusselt number distribution on the target surface.

The main objective of the present study is to simulate the fluid mechanics and mass transfer enhancement in separated and reattaching flow over a backward-facing step with local forcing. The large eddy simulation (LES) is employed to determine the characteristics of flow and mass transfer processes with local forcing.

Mathematical formulation

The calculations have been performed using a Navier-Stokes equations solver, which was developed between LETTM (Laboratoire d'Energétique et des Transferts Thermiques et Massiques, Tunisie) and LIMSI (Laboratoire d'Informatique pour la Mécanique et les Sciences de l'Ingénieur, Orsay Paris, France) for the simulation of complex flows.

The reasons of the choice of a 2-D approach are:

– the studied configuration is not a boundary layer situation, since the production of kinetic energy and turbulent momentum transfers take place starting from the outside and not from the wall; this will modify the exchange process,
– in their initial development from the point of separation, the shear layer and the recirculation are supposed to be dominated, by transverse structures that remain coherent, and
– it is supposed that if the transverse instabilities develop, the transverse component of vorticity ω_z is always stronger than ω_x and ω_y. Furthermore, has the example of the vortices of Görtler, even the instabilities are present, there is an effect of compensation on the parietal transfer type upwash-downwash due to ascents and descents of fluid described by Liu [14].

These approximations were used by [15]. In addition, in our work, the depth step is greater than 10*h*, where *h* is the height of the step (see fig. 1), which allows us to consider, according to Dumoulin [16], that the flow is 2-D.

Governing equations

The conservation equations describing the flow are the time-dependent, 2-D Navier--Stokes equations and the conservation equation for a constant-property incompressible fluid.

The principle of LES is to explicitly simulate the large scales of a turbulent flow while parameterizing the small scales. Therefore, one begins by filtering the Navier-Stokes equations to obtain an equation for the large-scale motion. As usual, the non-linearity of the Navier-Stokes equations makes it impossible to obtain an exact closed equation for any filtered quantity, meaning that a term analogous to the Reynolds-averaged Navier-Stokes (RANS) equations is produced and must be modelled.

For the flows considered here, the basic governing equations are written in dimensionless form as:

$$\frac{\partial \overline{u}_i}{\partial t} = 0$$

$$\frac{\partial \overline{u}_i}{\partial t} + \frac{\partial \overline{u}_i \overline{u}_j}{\partial x_j} = -\frac{\partial \pi}{\partial x_j} + \frac{\partial}{\partial x_j}\left(\frac{1}{\mathrm{Re}}\frac{\partial \overline{u}_i}{\partial x_j}\right) - \frac{\partial \tau_{ij}}{\partial x_j}$$

$$\frac{\partial \overline{C}}{\partial t} + \frac{\partial \overline{u}_j \overline{C}}{\partial x_j} = \frac{\partial}{\partial x_j}\left(\frac{1}{\mathrm{Re}\,\mathrm{Sc}}\frac{\partial \overline{C}}{\partial x_j}\right) - \frac{\partial (q_j)}{\partial x_j} + S_0$$

The governing dimensionless parameter appearing in the above equations are the Reynolds number (Re = U_0H/ν) and the Schmidt number (Sc = ν/D) based on the inlet average velocity (U_0) and the domain height (H). ν and D are, respectively, the kinetics viscosity and the mass diffusivity. S_0 represents the source term. In these equations, $\overline{u}_i$ and C are the filtered part, respectively, of the velocity and the concentration of mass substance. The modified pressure is given by $\pi = \overline{p} + 1/3\tau_{kk}$.

Subgrid scale model

The subgrid scale Reynolds stress is estimated by means of the eddy viscosity model τ_{ij} and the concentration turbulent flux q_j are based on the eddy-viscosity model approach, $\tau_{ij} = 2\nu_t \overline{S}_{ij}$ and $q_j = D_t(\partial \overline{C}/\partial x_j)$ where:

$$\overline{S}_{ij} = \frac{1}{2}\left(\frac{\partial \overline{u}_i}{\partial x_j} + \frac{\partial \overline{u}_j}{\partial x_i}\right)$$

is the strain rate tensor of the filtered flow field. The eddy diffusivity is generally related to eddy viscosity ν_t with the help of the turbulent Prandtl number ($\mathrm{Pr}_t = \nu_t/D_t = 0.6$).

Closure will be done when a model for the subgrid-scale (SGS) is chosen. Throughout this paper, we have chosen a mixed SGS model, which is a part of one parameter

(α) family of models proposed by Ta Phuoc [17] and Sagaut [18], and also used by Leonard *et al.* [19]. These models take into account both the large and the small scales.

The turbulent eddy viscosity is given by a non-linear combination of the second invariant of the shear stress tensor $|\bar{S}|$, the characteristic length scale Λ and the kinetic energy q_c^2 of the highest resolved frequencies:

$$\nu_t = c_m |\bar{S}|^{\alpha} (q_c^2)^{(1-\alpha)/2} \Lambda^{(1+\alpha)}$$

This can be viewed as a non-linear combination of the Smagorinsky [20] and the mixing-length model [21]. For α = 0 and 1, the mixing length and the Smagorinsky models are retrieved, respectively.

When considering homogeneous isotropic turbulence and α = 0.5 (the value retained throughout this work), the theoretical value of the parameter c_m is found equal to 0.04 on the basis of an equilibrium assumption between the dissipation and energy-transfer rates. The characteristic length scale is usually chosen to be $\Lambda = (\Delta x \Delta y)^{1/2}$, where Δx and Δy are mesh sizes in the x- and y-directions, respectively. The second invariant of the shear stress tensor is given by:

$$|\bar{S}| = \sqrt{\frac{\bar{S}_{ij}\bar{S}_{ij}}{2}}$$

and the kinetic energy q_c^2 is obtained by the scale similarity assumption and by means of a double-filtering technique: $q_c^2 = (1/2)(\bar{u}_i - \hat{\bar{u}}_i)^2$, where (^) represents a filter with a cut-off length of 2Λ. The explicit filter used here is a local weighted-average $\hat{\bar{u}}_i = (1/4)\bar{u}_{i-1} + (1/2)\bar{u}_i + (1/4)\bar{u}_{i+1}$.

The mixed SGS model is a self-adapted model, because the eddy viscosity vanishes automatically at the wall and in the regions of the flow where all the structures are well resolved.

Numerical procedure

The time integration is performed using a time-splitting algorithm, also known as a prediction-projection algorithm, which allows one to decouple pressure from velocity. Assuming all quantities known at time $n\Delta t$, the solution at time $(n + 1)\Delta t$ is obtained as follows.

An intermediate velocity field U^* is first computed using a second-order time scheme. This time stepping combines a second order backward Euler scheme for the diffusion terms, with an explicit second-order Adams-Bashforth extrapolation for the non-linear terms, taking into account known pressure field. This step reads:

$$\frac{3U^* - 4U^n + U^{n-1}}{2\Delta t} + 2(U\Delta U)^n - (U\Delta U)^{n-1} = -\Delta p^n + \frac{1}{\mathrm{Re}}\nabla^2 U^*$$

– In the second step, this intermediate velocity field is projected on to the subspace of divergence free vector field using the Helmholtz decomposition theorem. This step reads:

$$\frac{3(U^{n+1}-U^{*})}{2\Delta t}=-\nabla(\underbrace{p^{n+1}-p^{n}}_{\varphi})$$

– It is accomplished by taking the divergence of equation giving rise to a Poisson's type equation for the incremental pressure: $\Delta\varphi = (3/2\Delta t)\nabla U^*$.
– This equation is solved with a multigrid algorithm, in which the presence of internal blockings is automatically taken into account.
– Once the pressure field is obtained, the new quantities at $n + 1$ are given by:

$$\begin{cases} p^{n+1}=\varphi+p^{n} \\ U^{n+1}=U^{*}-\dfrac{2}{3}\Delta t\nabla\varphi \end{cases}$$

The space discretization uses a centred scheme for the diffusive fluxes and a second order upwind finite difference method by means of a quadratic upstream interpolation convective kinematics (QUICK) scheme for the convective terms, as proposed by Leonard [19].

Physical problem

Two-dimensional flow behind a backward-facing step subjected to a sinusoidal forcing is simulated. The computational domain and the co-ordinates system are represented in fig. 1. Channel expansion ratio is fixed at $H/h = 3$ in all the study, where H and h are the heights of the domain and the step, respectively. The Reynolds number is varied in the range of $10000 \leq \mathrm{Re} \leq 50000$ and the Schmidt number is fixed at 1. To control the flow, Chun *et al.* [5], and Yoshioka *et al.* [6], experimentally introduced a periodic forcing by pulsating jet (blowing and suction of the fluid) at the edge of the step. In this work, we have simulated such a forcing by introducing a local *velocity* $u = A\sin(2\pi ft)$ (fig. 1), where A and f are the amplitude and the frequency forcing, respectively. The mass source S is placed in the upstream of the step with a dimensionless concentration $C = 1$. At the channel inlet, a fully developed parabolic profile for the velocity is deployed. At the exit, convective boundary conditions for all variables ($\partial u/\partial x = \partial v/\partial x = \partial C/\partial x = 0$) are set. No-slip conditions are prescribed at the body surfaces ($u = v = 0$). At the upper boundaries, symmetry conditions simulating a frictionless wall are used $\partial u/\partial y = v = \partial C/\partial y = 0$. C is given as $C = (c - c_\mathrm{f})/(c_\mathrm{s} - c_\mathrm{f})$ where c_s is the concentration of mass source and c_f is that of the fluid.

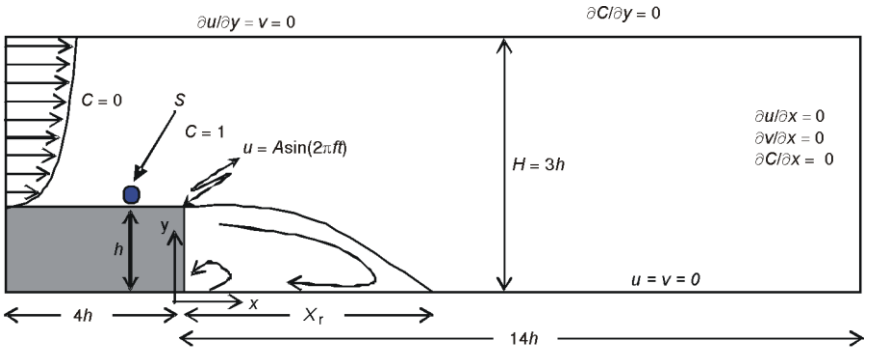

Figure 1. Geometric configuration and boundary layer

Results and discussion

Grid and time-step refinement

In this work, all refinement tests are undertaken on non-forcing flow.

The grid refinement tests have been performed using three uniform fine grids: 66 × × 33, 104 × 66, and 130 × 75 for Re = 33000. Results showed that when we pass from the first grid to the second, the reattachment length X_r/h undergoes an increase of 7.1%. When we pass from the second grid to the third, the reattachment length undergoes an increase of only 1.12%. We conclude that the grid of 104 × 66 gives a good compromise between precision and calculation time and is sufficient to carry out a numerical study of this flow.

The time-step Δt is conditioned by the Courant-Friedrich-Lewy (CFL) criterion. The adjustment of its value is undergone using the optimal 104 × 66 grid. Some preliminary runs showed that the dimensionless time interval tU_o/H = 400 is large enough to reach the asymptotic regime considered in the current study. Accordingly, we have done three simulations with Δt equal to $8\cdot10^{-3}$, $4\cdot10^{-3}$, and 10^{-3}. Obtained reattachment length values are X_r/h = 6.7, 7.2 (*i. e* an increase of 6.94% with respect to the previous value), and 7.28 (*i. e* an increase of only 1.1%), respectively. Basing on these data, and calculation-time consuming considerations, the time-step value is finally set to $4\cdot10^{-3}$. It's worth to remind here, that for $\Delta t = 10^{-3}$, 400000 time steps are necessary to reach the asymptotic regime. This number falls down to 100000 for $\Delta t = 4\cdot10^{-3}$.

Structure of non-controlled flow and test validation

Structure of the non-controlled flow

Figure 2 represents the average streamlines map of the mean flow for Re = 33000. We can clearly observe the development of a recirculation bubble formed by two vortical structures. The smaller vortex is located close to the lower step corner, and the main adjacent vortex is located immediately downstream. The large main vortex is limited above by the separating streamline which runs from the step edge down to the reattachment point (indicated in fig. 2. by a triangle). The same flow pattern was observed by Scharm *et al.* [22] and Bouda *et al.* [23]. The contours of the normal velocity component *v* are represented in the fig. 3. The negative contours are plotted using dashed lines and the positive contours using solid lines. The existence of negative *v* contours in the outer and downstream regions of the reattachment all around the recirculation bubble indicates that most of the flow is directed downward. This must be essentially due to the turbulent activity of the external big eddies towards the wall. In the reattachment region, we can observe also high values in the normal gradient of the *v* velocity component. Also, we can notice the presence of two counter-rotating vortexes in the recirculation bubble. This is in good agreement with the references [22, 23].

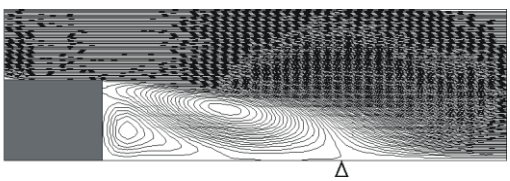

Figure 2. Average streamlines of the non-forcing mean flow, Re = 33000

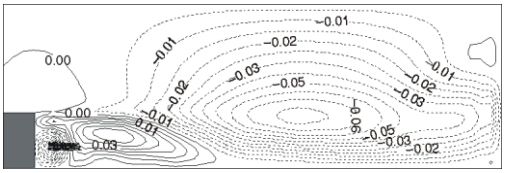

Figure 3. Contours of the longitudinal velocity component, Re = 33000

Test validation

For the purpose of validation of the present computational results, the flow without applied local forcing was validated, for different Reynolds number, against the benchmarked results of the recirculation region. In our simulations, the reattachment length for Re = 23000 and Re = 33000 are $X_r/h = 7$ and $X_r/h = 7.2$, respectively. Experimental results of Chun *et al.*, [2] are $X_r/h = 7.2$ and X_r/h=7.4. Errors committed are then 2.77% and 2.7% for Re = 23000 and Re = 33000, respectively. This shows a good agreement between the results.

Structure of controlled flow

The variation of the normalized reattachment length X_r/X_{ro} (X_{ro} is the reattachment length of non-controlled flow) is plotted in fig. 4. as a function of the forcing frequency (presented by a Strouhal number of the forcing, St = fh/U_o, based on the step height (h) and the inlet average velocity, U_0) for various Reynolds number at the forcing amplitude $A = 0.3U_o$. In all Re cases, the reattachment length first decreases with increasing St before it reaches a minimum at the optimum forcing frequency (in term of reduces the reattachment length) St = 0.25, and then increases again. It is known that the shear layer above the recirculation bubble is the seat of formation of coherent vortical structures. These vortices that are convecting downstream are responsible for the entrainment out of the recirculation bubble. By stimulating their growth through applying a local forcing, the increased shear layer growth rate leads to a significant reduction of the recirculation bubble size and, hence, a reduction in residence time. The maximum reduction is obtained at the optimum forcing frequency St = 0.25. This frequency is related to the shedding-type instability in the separated shear layer and is associated with the momentum exchange induced by the modulation of the separated shear layer [24]. We can observe also, for all forcing frequency, that the reduction ratio of the reattachment length increases with decreasing the Reynolds number. This shows that the control of reattachment length becomes more difficult by increasing the Reynolds number, because the energy brought by local forcing has a less significant effect by increasing this dimensionless number.

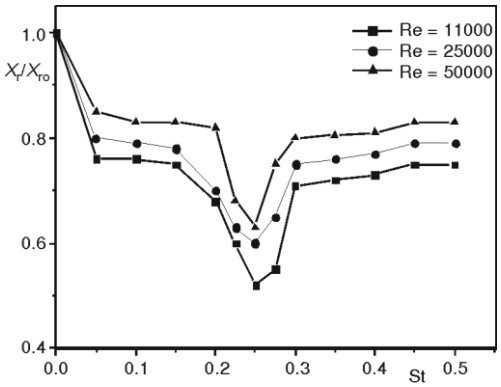

Figure 4. Normalized reattachment length X_r/X_{ro} against St for various Reynolds number, $A = 0.3U_o$

Table 1 enables us to compare the value of the optimum forcing frequency simulated in the present work by those of experimental and numerical investigations. This table shows an excellent agreement with these works.

The instantaneous isovalues of transversal velocity u and isovorticity are displayed for St = 0 (without control), St = 0.05, St = 0.25 (optimum forcing frequency), and St = 1 in fig. 5 at Re = 33000. We can observe clearly that the number of the vortical structures (dark zones for u-contours and clear zones for isovorticity) in the channel downstream of the step increases by local forcing. This is due to the change of the structure of recirculation bubble and the shedding process following the modification of the separation phenomenon of the

Table 1. Optimum forcing frequency for separated and reattaching flow

Authors	Re	Expansion ratio	Optimum St
Battacharjee *et al*. [3]	$2.6\text{-}7.6\cdot10^4$	1.1	0.2-0.4
Honami *et al*. [25]	$3.85\cdot10^4$	1.5	0.2
Chun *et al*. [2]	$1.3\text{-}3.3\cdot10^4$	1.5	0.25-0.275
Yoshioka *et al*. [6]	$1.8\text{-}5.5\cdot10^3$	1.5	0.18-0.22
Dejoan *et al*.* [26]	$1.8\text{-}5.5\cdot10^3$	1.5	0.2
*Present work**	$10^4\text{-}5\cdot10^4$	1.5	0.25

* Numerical works

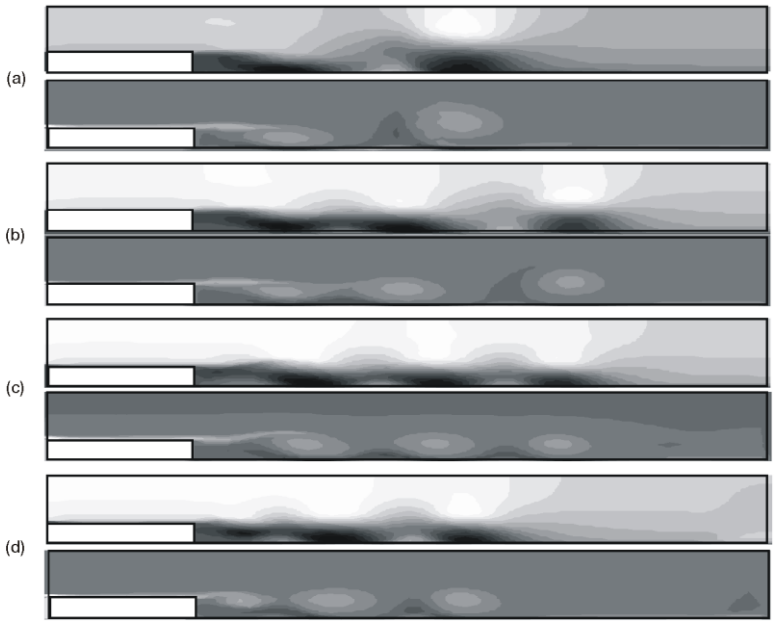

Figure 5. Isovalues of transversal velocity *u* (on the top) and isovorticity (on the bottom) at tU_o/H = 400 and Re = 33000. (a) St = 0 (non-controlled flow), (b) St = 0.05, (c) St = 0.25 (optimum), and (d) St = 1

boundary layer at the step edge. It is noted that the quantity of energy added to the flow by the local forcing makes the flow more active but that varies with the forcing frequency. The tab. 2 confirms the last idea, indeed the convection velocity u_c of the vortical structures downstream the step increases by control and reaches a maximum value at the optimum forcing frequency. According to Yoshioka *et al*. [6], the additional of the momentum transfer by the activated turbulent motion achieved by the induced periodic local forcing is responsible to the modifications observed in the flow structure.

Table 2. Convection velocity of vortical structures downstream the step

Forcing frequency (St)	0 (n. c.)	0.05	0.25 (o. f.)	1
Convection velocity (u_c)	$0.25U_o$	$0.44U_o$	$0.47U_o$	$0.4U_o$

n. c. – non-controlled; o. f. – optimum frequency

Mass transfer characteristics

Effect of forcing frequency

The simulated mass transfer rate, expressed by the local Sherwood number, Sh = $= -h(\partial C/\partial y)_{y=0}$, is plotted against the dimensionless longitudinal distance x/h for varying forcing frequency St in fig. 6 at $A = 0.3U_0$ and Re = 33000. The earlier studies [10, 11] established that the mass (or heat) transfer coefficient attains a maximum around the reattachment point, and decreases after this point. The overall profiles the Sherwood number fits the above general description. A closer inspection of the plots of fig. 6 that, for the forcing amplitude A fixed, the location of the maximum Sherwood number Sh_m moves upstream by control. The minimum location observed at optimum local forcing St = 0.25. This is compatible with the observation that the size of recirculation bubble is reduced. We can note also, the augmentation of the Sherwood number in the recirculation bubble by application of local forcing. The maximum enhancement of Sh is observed with the optimum forcing frequency. This can be explained by the modification of the shear layer in the vicinity of the sharp separation edge by the local forcing. This modification gives rise to a large increase in the entrainment close to the separation edge, which increases the shear layer growth rate. As a consequence, the size of recirculation decreases and the mass transfer, between the flow from the inlet and the wall, enhances.

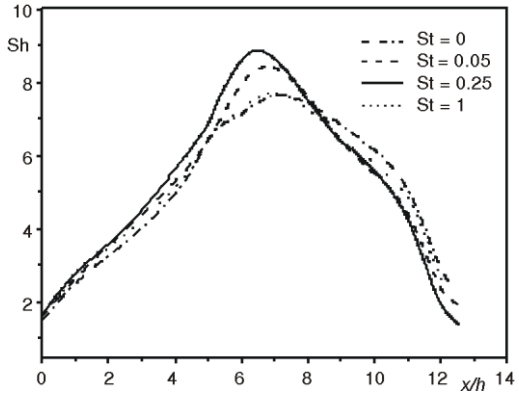

Figure 6. Profiles of Sherwood number Sh for various forcing frequency St, $A = 0.3U_0$ and Re = 33000

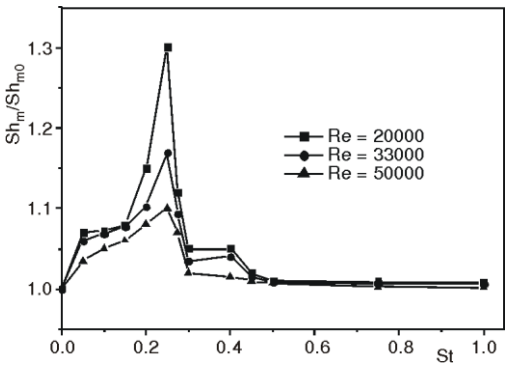

Figure 7. Normalized maximum Sherwood number Sh_m/Sh_{m0} against St for various Reynolds number, $A = 0.3U_0$

The normalized maximum Sherwood number Sh_m/Sh_{m0} (Sh_{m0} is the Sherwood number for non-controlled flow) against St for various Reynolds number at $A = 0.3U_0$ are represented in fig. 7. For all Reynolds number Sh_m increases by application of local forcing. The maximum is obtained at the optimum forcing frequency St = 0.25. It is noted also that the ratio Sh_m/Sh_{m0}, for all forcing frequency, becomes more important by decreasing the Reynolds number. This shows, for A fixed, that the enhancement of the mass transfer, by the local forcing downstream of backward step becomes less important by augmentation of Reynolds number.

Effect of forcing amplitude

The profiles of Sherwood number Sh are represented in fig. 8 for various forcing amplitude *A* while fixing the forcing frequency in the optimal value (St = 0.25) and the Reynolds number at 33000. With increasing the forcing amplitude, the augmentation of Sh, within the separation bubble, becomes discernible. The enhancement of Sh is more pronounced in the vicinity of reattachment point. After the reattachment point is passed, Sh decreases faster with increasing the forcing amplitude. It is noted also that the location of the maximum mass transfer shifts toward the step and the maximum Sherwood number Sh_m enhances by increasing the forcing amplitude. Physically, as the forcing effect increases, the entrainment of the high-energy fluid outside of the recirculation bubble becomes more vigorous by the action of the intensified recirculating flow driven by the motion of the large-scale vortex. This causes a substantial augmentation of mass transfer, especially around the reattachment point [11].

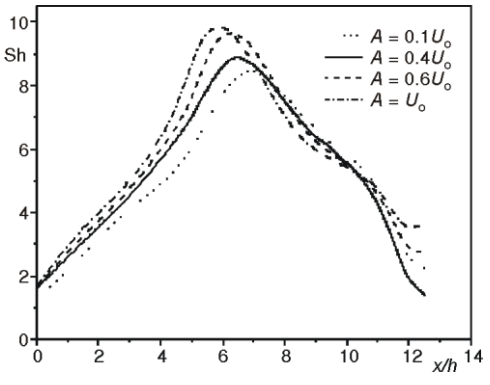

Figure 8. Sherwood number profiles for various forcing amplitude at St = 0.25 and Re = 33000

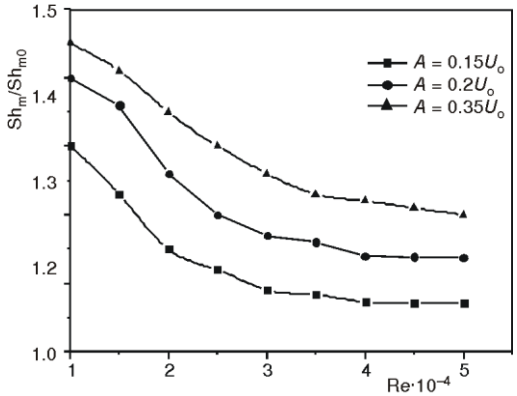

Figure 9. Normalized Sherwood number Sh_m/Sh_{m0} against Re for different forcing amplitude *A*

For testing the effectiveness of the control on the mass transfer, the ratio Sh_m/Sh_{m0} against the Reynolds number is plotted in fig. 9 for various forcing amplitude at St = 0.25. For all *A* Sh_m/Sh_{m0} decreases by increasing the Reynolds number. It is seen also, for all Re, that the ratio Sh_m/Sh_{m0} increases by increasing the forcing amplitude. These results suggest that the enhancement of the mass transfer observed at the optimum forcing frequency can be improved by augmentation of the forcing amplitude or/and by reduction of Reynolds number.

To sum up, the overall convective mass transfer rate is found to increase when the local forcing is imposed. It is worth pointing out that this finding is analogous to the case of heat transfer [10, 27].

Conclusions

Large eddy simulation was performed to portray the flow and mass transfer characteristics in the separated and reattaching flow. By introduction of periodic local forcing on the separation point, principal changes in flow characteristics are observed. The number and the convection velocity, of the vortical structures downstream the step, are enhanced. The reattachment length, for all Reynolds number, is reduced measurably. The largest reduction is

observed at the optimum forcing frequency, St = 0.25. The general pattern of Sherwood number profiles indicates that the mass transfer reaches a maximum around the reattachment point. The location of maximum Sherwood number is shifted upstream and the mass transfer in the recirculation bubble enhanced by the imposed forcing. These effects are noticeable as the forcing amplitude increases at the optimum forcing frequency. The influence of the periodic local forcing weakens by increasing the Reynolds number.

Nomenclature

A – forcing amplitude, [ms^{-1}]
C – dimensionless concentration [= $(c - c_f / c_s - c_f)$]
c – concentration, [molL^{-1}]
D – mass diffusivity, [m^{2}s^{-1}]
D_t – eddy diffusivity, [m^{2}s^{-1}]
f – forcing frequency, [Hz]
H – computational domain width, [m]
h – step height, [m]
Pr_t – turbulent Prandtl number, [–]
p – pressure, [Pa]
q_c^2 – kinetic energy, [J]
q_j – concentration turbulent flux, [molm^{-2}s^{-1}]
Re – Reynolds number (= $U_o H/\nu$), [–]
$\bar{S}$ – shear stress tensor
$\bar{S}_{ij}$ – strain rate tensor
Sc – Schmidt number (ν/D), [–]
Sh – Sherwood number [= $(-h(\partial C/\partial y)_{y=0}$], [–]
Sh_m – maximum Sherwood number, [–]
St – Strouhal number (= fh/U_o), [–]
U_o – inlet average velocity, [ms^{-1}]
u – longitudinal velocity, [ms^{-1}]
u_c – convection velocity, [ms^{-1}]
u_i – velocity vector, [ms^{-1}]
v – transversal velocity, [ms^{-1}]
X_m – maximum mass transfer abscissa, [m]
X_r – reattachment length, [m]
x, y – Cartesian co-ordinates

Greek symbols

Λ – characteristic length scale
ν – kinematic viscosity, [m^{2}s^{-1}]
ν_t – turbulent viscosity, [m^{2}s^{-1}]
π – modified pressure, [Pa]
τ_{ij} – subgrid tensor

Subscripts

f – fluid
s – source
o – non-controlled case

References

[1] Sigurdson, L. W., The Structure and Control of a Turbulent Reattaching Flow, *J. of Fluid Mechanics*, *298* (1995), 1, pp.139-165
[2] Chun, K. B., Sung, H. J., Control of Turbulent Separated Flow over a Backward-Facing Step by Local Forcing, *Exp. Fluids*, *21* (1996), pp. 417-426
[3] Bhattacharjee, S., Scheelke B., Troutt, T. R., Modification of Vortex Interaction in a Reattaching Seperated Flow. *AIAA*, *24* (1986), 4, pp. 623-629
[4] Kiya, M., Shimizu, M., Mochizuki, O., Sinusoidal Forcing of a Turbulent Separation Bubble, *J. of Fluid Mechanics*, *342* (1997), 1, pp. 119-139
[5] Chun, K.B., Sung, H. J., Visualization of a Locally-Forced Separated Flow over a Backward-Facing Step, *Exp.Fluids*, *25* (1998), 2, pp. 417-426
[6] Yoshioka, S., Obi., S., Masuda, S., Organized Vortex Motion in Periodically Perturbed Turbulent Flow over a Backward-Facing Step, *Int. J. Heat Fluid Flow*, *22* (2001), 3, pp. 301-307
[7] Uruba, V., Jonas, P., Mazur, O., Control of a Channel-Flow behind a Backward-Facing Step by Suction/Blowing. *Int. J. of Heat and Fluid Flow*, *28* (2007), 4, pp. 665-672
[8] Oyakawa, K., *et al*., Heat Transfer Control by Using Jet Discharge in Reattachment Region Downstream of a Backward-Facing Step, *International Communications in Heat and Mass Transfer*, *22* (1995), 3, 343-352
[9] Velazquez, A., Arias, J. R., Mendez, B., Laminar Heat Transfer Enhancement Downstream of a Backward Facing Step by Using a Pulsating Flow, *Int. J. Heat Mass Transfer, 51* (2008), 7-8, pp. 2075-2089
[10] Mehrez, Z., *et al*., The Influence of the Periodic Disturbance on the Local Heat Transfer in Separated and Reattached Flow, *Journal of Heat and Mass Transfer, 46* (2009), 1, pp. 107-112

[11] Hwang, K. S., Sung, H. J., Hyun, J. M., Flow and Mass Transfer Measurements for a Flat Plate of Finite Thickness in Pulsating Flow, *Int. J. of Heat and Mass Transfer, 41* (1998), 18, pp. 2827-2836
[12] Younsi, M., Computational Analysis of MHD Flow, Heat and Mass Transfer in Trapezoidal Porous Cavity, *Thermal Science, 13* (2009), 1, pp. 13-22
[13] Xu, P., *et al*., Heat Transfer under a Pulsed Slot Turbulent Impinging Jet at Large Temperature Differences, *Thermal Science, 14* (2010), 1, pp. 271-281
[14] Liu, J. T. C., Lee, K., On the Growth of Mushroomlike Structures in Nonlinear Spatially Developing Gertler Flow, *Phys. Fluids A-Fluid, 4* (1992), 1, pp. 95-l 03
[15] Giovannini, A., Marcos, V. B., Heat Transfer in Vicinity of Reattaching Point over a Backward Facing Step (in French), *Rev Gén Therm, 37* (1997), 2, pp. 89-102
[16] Dumoulin, J., Characterisation of the Flow over a Backward Facing Step: Test Case n°1 (in French), *2568.00/CERT/DERMES.*, ONERA, France, 1996
[17] Ta Phuoc, L., Subgrid Models Applied for Unsteady Separated Flows (in French), *Proceedings*, DRET Conference: Turbulent Unsteady Aerodynamics – Numerical and Experimental Aspects, Paris, France, DGA/DRET editiors, 1994
[18] Sagaut, P., Large Eddy Simulation for Incompressible Flows: An Introduction, Book Math., Springer
[19] Leonard, B. P., Simple High Accuracy Resolution Program for Convection Modelling of Discontinuities, *Int. J. for Num. Methods in fluids, 8* (1988), 10, pp. 1291-1318
[20] Smagorinsky, J. S, General Circulation Experiment with the Primitive Equation I, The Basic Experiment, *Mon. Weather Rev. 91* (1963), 3, pp. 99-164
[21] Germano, M., *et al*., A Dynamic Subgrid Scale Eddy Viscosity Model, *Phys. Fluids A., 3* (1991), 7, pp. 1760-1765
[22] Scharm, C., Rambaud, P., Riethmuller, M. L., Wavelet Based Eddy Structure Deduction from a Backward Facing Step Flow Investigation Using a Particle Image Velocimetry. *Exp. Fluids*, 36 (2004), 2, pp. 233-245
[23] Bouda, N. N., *et al*., Experimental Approach and Numerical Prediction of Turbulent Wall Jet over a Backward Facing Step. *Int. J. of Heat and Fluid Flow, 29* (2008), 4, pp. 927-944
[24] Nagib, H. M., Reisenthel, P. H., Koga, D. J., On the Dynamical Scaling of Forced Unsteady Separated Flows, AIAA Shear Flow Control Conference, Boulder, Col., USA, AIAA paper No. 85-0553, 1985
[25] Honami, S., Shizawa, T., Tsuchitani, H., Organized Structures in the Reattachment Process in a Backward-Facing Step Flow, *Proceeding*, 9th Symposium on Turbulent Shear Flow, Kyoto, Japan,, 1993, p. 108
[26] Dejoan, A., Leschziner, M. A., Large Eddy Simulation of Periodically Perturbed Separated Flow over a Backward-Facing Step. *International Journal of Heat and Fluid Flow, 25* (2004), 4, pp. 581-592
[27] Hourigan, K., *et al*., Augmented Forced Convection Heat Transfer in Separated Flow Around a Blunt Flat Plate, *Experimental Thermal and Fluid Science, 4* (1991), 2, pp. 82-91

Paper submitted: October 27, 2009
Paper revised: March 16, 2010
Paper accepted: August 21, 2010